Soot Formation in Laminar Premixed Ethylene/Air Flames at Atmospheric Pressure

F. XU, P. B. SUNDERLAND,* AND G. M. FAETH†
Department of Aerospace Engineering, The University of Michigan, Ann Arbor, Michigan 48109-2118

Soot formation was studied within laminar premixed ethylene/air flames (C/O ratios of 0.78–0.98) stabilized on a flat-flame burner operating at atmospheric pressure. Measurements included soot volume fractions by both laser extinction and gravimetric methods, temperatures by multiline emission, soot structure by thermophoretic sampling and transmission electron microscopy, major gas species concentrations by sampling and gas chromatography, concentrations of condensable hydrocarbons by gravimetric sampling, and velocities by laser velocimetry. These data were used to find soot surface growth rates and primary soot particle nucleation rates along the axes of the flames. Present measurements of soot surface growth rates were correlated successfully by predictions based on typical hydrogen-abstraction/carbon-addition (HACA) mechanisms of Frenklach and co-workers and Colket and Hall. These results suggest that reduced soot surface growth rates with increasing residence time seen in the present and other similar flames were mainly caused by reduced rates of surface activation due to reduced H atom concentrations as temperatures decrease as a result of radiative heat losses. Primary soot particle nucleation rates exhibited variations with temperature and acetylene concentrations that were similar to recent observations for diffusion flames; however, nucleation rates in the premixed flames were significantly lower than in the diffusion flames for reasons that still must be explained. Finally, predictions of yields of major gas species based on mechanisms from both Frenklach and co-workers and Leung and Lindstedt were in good agreement with present measurements and suggest that H atom concentrations (relevant to HACA mechanisms) approximate estimates based on local thermodynamic equilibrium in the present flames.

NOMENCLATURE

A	pre-exponential factor
A_v	Avogadro's number
C_{HACA}	coefficient in HACA growth mechanism
C_i	carbon mass per mole of species i
d_p	mean primary soot particle diameter
E	activation energy
f_s	soot volume fraction
$[i]$	molar concentration of species i
k_g	soot particle surface growth rate constant
k_i	reaction rate coefficient of reaction i
k_n	soot primary particle nucleation rate constant
M_i	molecular weight of species i
n	power of temperature dependence of pre-exponential factor, reaction order
n_p	number of primary particles per unit volume
R_i	terms of the HACA soot surface growth rate formulas
S	soot particle surface area per unit volume
t	time
T	temperature
u	streamwise velocity
$\bar{v}_i$	mean molecular velocity of species i
w_g	soot particle surface growth rate
w_n	soot primary particle nucleation rate
X_i	mole fraction of species i
z	streamwise distance

Greek Symbols

α_i	empirical (steric) factor in HACA soot surface growth rate formulas
η	collision efficiency
ρ	gas density
ρ_s	soot density

* Present address: NASA Lewis Research Center, Cleveland, OH 44135.
† Corresponding author.

COMBUSTION AND FLAME 108:471–493 (1997)

Published by Elsevier Science Inc.

0010-2180/97/$17.00
PII S0010-2180(96)00200-3

Subscripts

CH	refers to mechanism of Colket and Hall [37]
FW	refers to mechanism of Frenklach and co-workers [33–35]
max	maximum value in flame

INTRODUCTION

Soot is present in most nonpremixed hydrocarbon/air flames, where it affects flame reaction mechanisms and structure. As a result, soot processes must be understood in order to achieve effective methods of computational combustion and predictions of flame radiation and pollutant emissions. Motivated by these observations, the main objectives of the present investigation were to extend earlier studies of soot processes in laminar diffusion flames, due to Sunderland and co-workers [1–3], to laminar premixed flames, emphasizing processes of soot growth and nucleation.

Soot processes in flame environments have been reviewed by Haynes and Wagner [4], Glassman [5] and Howard [6]; therefore, the following discussion of past work will be brief. Representative recent studies of soot processes in laminar premixed flames and other configurations where the effects of fuel/oxidant mixing are small, include Bockhorn and co-workers [7–10], Harris et al. [11–17], Ramer et al. [18], Wagner and co-workers [19–23], Howard and co-workers [24–28], Macadam et al. [29], Smedley et al. [30], D'Alessio and co-workers [31, 32], and references cited therein. Most of the mass of soot and associated heavy hydrocarbons is thought to come from C_2H_2, which generally is the most abundant gaseous hydrocarbon in regions where soot is formed in premixed flames. It is also thought that reaction of C_2H_2 to form soot occurs in one of two ways: (1) by reactive addition of C_2H_2 to growing and coalescing polycyclic aromatic hydrocarbons (PAH) that eventually either become soot nuclei or reactively coalesce at the surface of growing soot particles, and (2) by the direct reactive addition of C_2H_2 to the surface of growing soot particles. Currently, however, there is considerable uncertainty about the relative contributions of these two mechanisms to soot formation for given flame conditions [6, 24–37]. Past observations have also shown that soot particles become less reactive for soot surface growth with increasing residence time (age) in laminar premixed flames. Frenklach and Wang [33] proposed that this reduced reactivity to soot growth is caused by reduced concentrations of H as flow temperatures decrease due to radiative heat losses to the surroundings, because reactions between H and either the surface of soot particles or gaseous hydrocarbon molecules are needed to activate sites for carbon addition reactions. These features have been explained by models incorporating concepts of hydrogen-abstraction/carbon-addition (HACA) processes developed by Frenklach and co-workers [33–36] and subsequently extended by others, e.g., Colket and Hall [37] and Mauss et al. [10, 38]. Nevertheless, there are concerns about the data base involving laminar premixed flames that was used to develop and evaluate these models. For example, residence times in the laminar premixed flames generally were only estimated rather than measured, which compromises estimates of rate processes. In addition, soot structure in the laminar premixed flames generally was only approximated by equivalent spherical particles, rather than treated as aggregates of spherical primary soot particles that actually are observed in flame environments, which compromises estimates of important structural features of soot (e.g., surface-to-volume ratios) [39]. Finally, approximations of equivalent spherical particles that have not been very successful for representing the optical properties of soot [40–42] were used for nonintrusive estimates of soot structure properties during some studies.

Improved measurements of residence times and soot structure properties have been used during recent studies of soot processes in laminar diffusion flames [1–3]. In particular, residence times were found from velocity measurements using laser velocimetry, and soot structure properties were found using thermophoretic sampling and analysis by transmission electron microscopy (TEM) as discussed by Dobbins and Megaridis [43] and Rosner et al. [44]. These studies also involved measurements of temperatures and soot and gas con-

centrations that are needed to interpret soot nucleation and growth rates. The new measurements showed that soot growth rates in diffusion flames were comparable to growth rates observed for new soot in premixed flames [8–18], with no measurable effect of age. In addition, soot formation in diffusion flames was associated with the presence of C_2H_2, similar to observations in premixed flames [7–32], although effects of hydrocarbons other than C_2H_2 were also observed [3]. Resolving effects of age and various hydrocarbons on soot processes by measurements in laminar diffusion flames represents a challenging task, however, due to the complexity of transport processes in diffusion flames.

In view of this status, the objectives of the present investigation were to apply the experimental techniques developed during the laminar diffusion flame studies of Refs. 1–3 to study soot processes in laminar premixed flames, emphasizing flame and soot structure as well as processes of soot growth and nucleation. Existing theories of soot processes in flames, due to Frenklach and co-workers [33–36], Colket and Hall [37], and Leung et al. [45, 46], were used to help interpret and correlate the new measurements, considering both concentrations of gas species in the soot-formation region and soot growth rates. The test conditions were limited to fuel-rich laminar premixed ethylene/air flames at atmospheric pressure, similar to the flames studied by Harris and Weiner [11].

EXPERIMENTAL METHODS

Apparatus

The test flames were produced by a 60 mm diameter water-cooled porous-plate laminar premixed flat-flame burner directed vertically upward at atmospheric pressure (McKenna Products, Inc., high-pressure shroud model). The reactant mixture at the burner exit was surrounded by a 6 mm wide annular nitrogen flow to eliminate peripheral diffusion flames that are present when fuel-rich premixed flames are burned at room air. The flames were stabilized by impinging the burner flow on a flat plate, having a 30 mm diameter hole at the axis, that was located 32 mm above the burner exit. Room disturbances were controlled by surrounding the flames with layers of screens and a plastic enclosure.

Ethylene (polymer grade, 99.9% purity), dry air (dew point less than 240 K), and nitrogen (prepurified grade, 99.98% purity) were supplied to the burner. The fuel, nitrogen, and air flows were measured with rotameters that were calibrated with wet-test meters. The fuel and air flows were manifolded together and then passed through a line having a length-to-diameter ratio of roughly 1000 in order to obtain a properly premixed room temperature reactant flow at the burner inlet. Combustion products were removed using a blower whose 125 mm diameter inlet was located 700 mm above the stabilizing plate. The burner was cooled using water at room temperature (294 $\pm$ 2 K) with a flow rate sufficiently high that the coolant temperature rise was negligible.

The burner assembly could be traversed in the horizontal direction with a positioning accuracy of 100 μm, using a stepping-motor-driven linear positioner, and in the vertical direction with a positioning accuracy of 200 μm, using a laboratory jack, in order to accommodate rigidly mounted optical diagnostics.

Instrumentation

The following properties were measured along the axes of the test flames: soot volume fractions, soot primary particle diameters, soot temperatures, concentrations of major gas species, concentrations of condensable hydrocarbon species (CHS), and gas velocities. These measurements were used to find soot surface area per unit volume, the concentration of primary soot particles, soot surface growth rates, and primary soot particle nucleation rates.

Soot volume fractions were measured using both optical and gravimetric methods. The optical determinations of soot volume fractions involved deconvoluting laser-extinction measurements at 632.8 nm for chord-like paths through the flames, similar to earlier work [1–3]. The laser extinction measurements were reduced assuming that soot optical properties satisfied the small-particle (Rayleigh) scatter-

ing approximation, which was justified because scattering was small for present test conditions. Refractive indices needed to find soot volume fractions were taken from Dalzell and Sarofim [47], similar to past work [1–3]. Recent work has alleviated past concerns about the ex situ methods used by Dalzell and Sarofim [47]; see Wu et al. [48]. The experimental uncertainties of these measurements (95% confidence) are estimated to be less than 10% for $f_s > 0.1$ ppm, increasing inversely proportional to f_s for smaller soot volume fractions.

Soot volume fractions were also measured gravimetrically, similar to Howard and coworkers [24–26]. This involved isokinetic sampling from the flames followed by measurement of the gas and soot volumes in the samples. A 4 mm inner diameter (ID) quartz probe, aligned with the flow direction, was used for sampling. Samples were passed through a cold trap, primary and secondary filters, and into an evacuated gas collecting tank. The cold trap was a 4 mm ID glass tube, 200 mm in length, surrounded by an ice-water bath. Both filters were 47 mm in diameter (Gelman Part No. 66143, 200 nm, TF200, PTFE membrane). Sampling times were approximately 15 min to allow for collection of sufficient amounts of soot. The gas volume of each sample was determined by measuring the pressure rise over a timed interval for the collecting tank (which had a known volume); these results were verified by measurements of gas flow rates using a rotameter for some conditions, finding differences between the two methods less than 5%. Soot and CHS were extracted from the sample gas in the cold trap and filters. The CHS were subsequently removed using liquid dichloromethane (CH_2Cl_2). The filters and loose soot collected were then dried and weighed to determine the mass of soot in the sample. The soot volume was found assuming a soot density of 1850 kg/m^3 [1–3]. This information, along with the sample gas volume (corrected to flame conditions), yielded the gravimetric soot volume fraction with experimental uncertainties (95% confidence) less than 15%.

Soot primary particle diameters were measured using thermophoretic sampling and analysis by TEM similar to Refs. 1–3. Effects of soot aggregate size cause negligible sampling bias for present test conditions [44]. Primary particle diameters were nearly monodisperse at a given position (standard deviations were less than 10% of the mean). Experimental uncertainties (95% confidence) of these diameters were dominated by finite sampling limitations and were less than 10%. The number of primary soot particles per unit volume was then computed from the optically determined soot volume fraction, as follows:

$$n_p = 6f_s/\left(\pi d_p^{\,3}\right). \tag{1}$$

The resulting experimental uncertainties (95% confidence) of n_p are less than 32% for $f_s > 0.1$ ppm, increasing roughly inversely proportional to f_s for smaller values of soot volume fractions.

Temperatures were found within the soot-containing regions of the flame using multiline emission measurements, similar to Refs. 1–3. This involved deconvoluting spectral radiation intensities for chord-like paths through the flames and finding temperatures from measurements at three line pairs: 600/750, 700/830, and 600/830 nm. Temperature differences between the average and any of the line pairs were less than 30 K along the axes of the flames, while experimental uncertainties (95% confidence) of these measurements are estimated to be less than 50 K.

Concentrations of major gas species were measured by isokinetic sampling and gas chromatography similar to Refs. 1–3. A radiatively cooled stainless steel sampling probe having a port diameter of 2.1 mm was used. Gas species considered in the analysis included N_2, Ar, O_2, CO_2, CO, H_2O, H_2, CH_4, C_2H_2, C_2H_4, and C_2H_6. Experimental uncertainties of these measurements were less than 15% for mole fractions greater than 0.5%.

The concentrations of CHS were measured using the same sampling probe and filter/trap system as the gravimetric determination of soot volume fractions. The CHS that was extracted from the sampling system and filters by CH_2Cl_2 was weighed after removing the soot by filtering and the solvent by evaporation. No attempt was made to chemically characterize the CHS; instead it is reported on a volumetric basis. A molecular weight of 276 kg/kg-mol was as-

sumed for CHS concentrations because this approximates the molecular weight of condensable soot precursors found in the soot inception region of laminar diffusion flames by Dobbins et al. [49], which generally is dominated by the stabilomer soot precursor species identified by Stein and Fahr [50]. Experimental uncertainties (95% confidence) of these measurements, excluding the uncertainty of the mean molecular weight of CHS species, are estimated to be less than 30%.

Streamwise velocities were measured along the flame axes using laser velocimetry (LV) based on a dual-beam forward-scatter arrangement with the flow seeded with aluminum oxide particles, similar to Refs. 1–3. Experimental uncertainties (95% confidence) of streamwise velocities are estimated to be less than 5%, dominated by calibration uncertainties, with similar uncertainties of flame residence times computed using these data.

Test Conditions

Five premixed ethylene/air flames were studied, having atomic carbon/oxygen (C/O) ratios in the range 0.78–0.98, as summarized in Table 1. These flames roughly corresponded to the conditions of Harris and Weiner [11]; in addition, Benish et al. [28] recently report measurements for a premixed ethylene/air flame having a C/O ratio of 0.79, which represents conditions nearly identical to the flame having a C/O ratio of 0.78 considered during the present study. Maximum soot volume fractions for the present flames were in the range 0.2–0.8 ppm, which provided reasonable sensitivity for soot concentration measurements without excessive soot deposition on sampling probes. All five test flames were used for measurements of the concentrations of major gas species; however, three of the flames (C/O ratios = 0.78, 0.88, and 0.98) were studied more completely in order to find soot growth and nucleation properties.

COMPUTATIONAL METHODS

General Description

Predictions of flame properties based on the models of Frenklach and co-workers [33–35] and Leung and co-workers [45, 46] were used to supplement and to help interpret the present measurements. These predictions were obtained using PREMIX, the steady, laminar one-dimensional premixed flame computer program of Kee et al. [51]. PREMIX involves consideration of mixture-averaged multicomponent diffusion, thermal diffusion, and variable thermophysical and transport properties. Effects of radiative heat losses and chemical energy release were handled by using the

TABLE 1

Summary of the Test Flames[a]

C/O Ratio	0.78	0.83	0.88	0.93	0.98
Fuel-equivalence ratio	2.34	2.49	2.64	2.79	2.94
CO fuel-equivalence ratio	1.56	1.66	1.76	1.86	1.96
Fuel flow rate (mg/s)	30.8	32.4	34.1	35.7	28.9
Air flow rate (mg/s)	194.3	192.6	190.9	189.2	145.5
Reactant velocity (mm/s)[b]	68.4	68.4	68.4	68.4	53.1
Reactant composition (% by vol.)					
C_2H_4	14.0	14.8	15.6	16.3	17.0
O_2	18.0	17.8	17.7	17.5	17.4
$N_2 + Ar + CO_2$	68.0	67.4	66.7	66.2	65.6

[a] Premixed ethylene/air flames using a 60 mm diameter water-cooled flat-flame burner with 6 mm wide annular nitrogen coflow (McKenna Products Inc., high-pressure shroud standard model), constant water flow rate of 9.1 g/s, and constant nitrogen coflow rate of 165.6 mg/s (nitrogen burner exit velocity of 125.2 mm/s). Ambient pressure and temperature of 98.7 kPa and 294 ± 2 K. Gas properties: ethylene = polymer grade, 99.9% purity; dry air = dewpoint < 240 K; nitrogen = prepurified grade, 99.98% purity.

[b] Computed for ambient pressure and temperature conditions at burner exit.

present measurements to prescribe temperature and velocity distributions as functions of distance from the burner. The computations were evaluated using present measurements of the concentrations of major gas species.

The prescription of flow temperatures for the computations was straightforward in the region where soot was present and multiline temperature measurements were available. It was necessary, however, to estimate temperature distributions in the soot-free regions near the burner surface in order to complete the calculations. This was done by linearly extrapolating the measured temperature distributions to the burner surface, assuming the surface temperature of the porous burner to be 400 K. It was found that predictions of compositions in the soot-formation region were not significantly altered, however, when other reasonable near-burner temperature distributions (with burner surface temperatures of 300–800 K) were imposed.

Computations

Present calculations were carried out using 160 spatial increments for flames extending up to 35 mm from the burner exit. Grid spacing was adaptive so that spacing was up to five times tighter in regions where properties were changing rapidly. Absolute and relative convergence tolerances less than 10^{-5} were specified for the Newton iterations and time stepping. Doubling the number of grid points and halving the tolerances had negligible effects on predictions, i.e., concentration changes were less than 0.1%.

Chemical Mechanisms

The main objectives of present computations were to assess capabilities for estimating concentrations of major gas species and to provide estimates of small radicals such as H, O, and OH. Thus, the complete soot formation mechanisms of existing models [33–35, 45, 46] were not considered. As a result, the mechanism of Frenklach and co-workers [33–35] only included steps needed to describe reactions involving hydrocarbons up to C_6H_6; namely, 250 reversible elementary reactions involving 52 species. Similarly, the mechanism of Leung and co-workers [45, 46] was limited to hydrocarbons up to C_6H_6 and included 451 reversible reactions involving 87 species. Original sources and references cited therein should be consulted for the details of these mechanisms.

The present measurements were also used to evaluate proposed mechanisms of soot surface growth; the details of these mechanisms and computations will be discussed later.

RESULTS AND DISCUSSION

Soot Structure

Typical TEM photographs of soot samples collected in the present test flames are shown in Figs. 1 and 2. These results were obtained along the axis of C/O = 0.78 flame at 12.5 and 22.5 mm above the burner exit, respectively, which correspond to conditions near the beginning and end of soot formation. The present soot is typical of soot found in flames, consisting of roughly spherical primary soot particles having nearly constant diameters at a particular location, collected into aggregates having widely varying numbers of primary particles

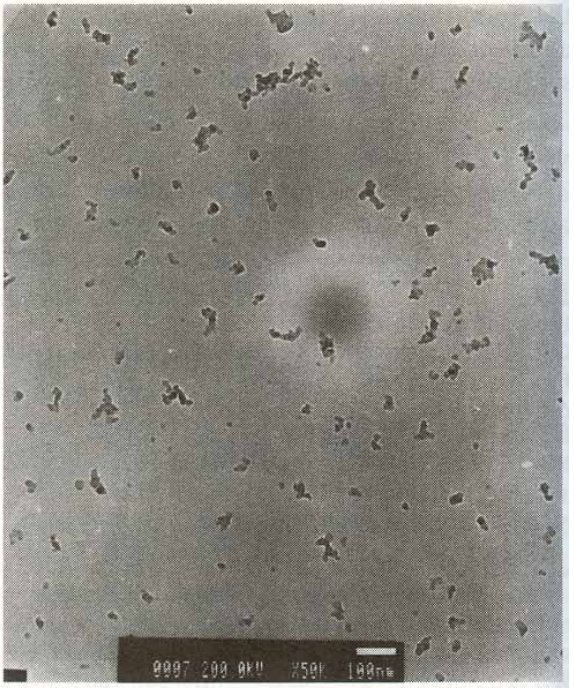

Fig. 1. TEM photograph of soot aggregates along the axis of the C/O = 0.78 flame at z = 12.5 mm.

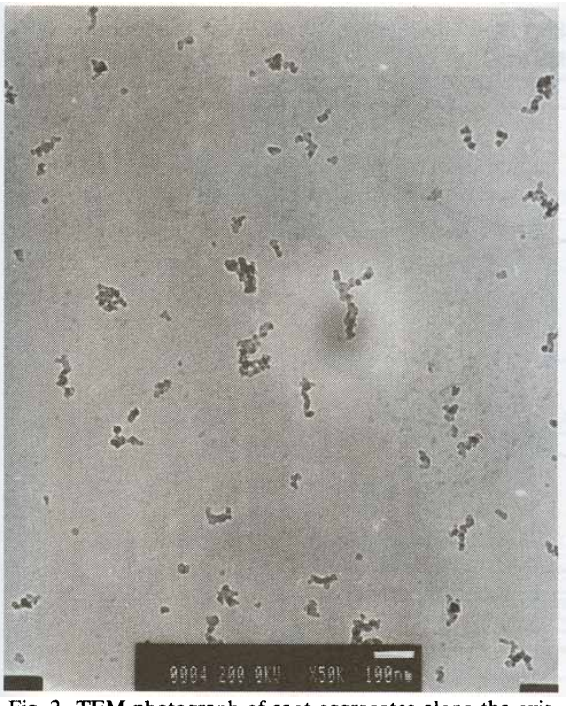

Fig. 2. TEM photograph of soot aggregates along the axis of the C/O = 0.78 flame at z = 22.5 mm.

per aggregate [1–6, 39–44]. The mean diameters of primary particles ranged up to 40 nm for present test conditions, increasing with increasing residence time and propensity to soot (increasing C/O ratio). The degree of aggregation, characterized by the mean number of primary particles per aggregate, increased similar to d_p with increasing residence time and propensity to soot.

In addition to the soot aggregates observed in Figs. 1 and 2, other relatively large translucent objects were observed on the TEM grids. These objects might be related to the soot precursor particles observed by Wersborg et al. [39] and D'Alessio and co-workers [31, 32] near soot inception conditions in laminar premixed flames; however, the objects observed in the present flames were much larger than the 2–3 nm diameter particles reported in Refs. 31, 32, and 39. Instead, these translucent objects consisted of roughly round single particles having varying and larger diameters (on the order of 100 nm) and poorer contrast as TEM images than primary soot particles. Evolution of these translucent objects into primary soot particles is not easily explained by dehydrogenation because anticipated density increases through dehydrogenation still would yield objects larger than the present primary soot particles. Other possibilities include liquid drops that are not spherical but instead wet and spread along the surface of the TEM grid, dropwise condensation of hydrocarbon vapors on the TEM grid, and some fault of the TEM grids themselves. These issues were not resolved during the present investigation, but they clearly merit additional study; fortunately, the numbers of translucent objects were relatively small compared to the numbers of primary soot particles in the flame regions studied during the present investigation.

Flame Structure

Measurements of temperatures, velocities, soot volume fractions, primary soot particle diameters, and the concentrations of major gas species along the axes of flames having C/O = 0.78, 0.88, and 0.98 are plotted as a function of height above the burner exit in Figs. 3–5. Corresponding residence times found by integrating the velocity measurements are shown at the top of the plots. The residence times are relative to the first position where finite soot volume fractions were measured.

Effects of buoyancy were significant for the present test conditions, so that streamwise velocities in Figs. 3–5 rapidly increase from burner exit values to roughly 1 m/s at z = 27.5 mm. These velocity increases slow variations of flame properties with increasing distance because residence-time increments are inversely proportional to velocities.

The presence of significant soot concentrations in the present flames causes significant radiative heat losses. These heat losses cause soot temperatures in Figs. 3–5 to decrease from 1900–2100 K (at z = 7.5 mm) to values of 1500–1600 K at the highest location where temperatures were measured (at z = 27.5 mm). Temperatures are generally higher at lower C/O ratios, due to more favorable stoichiometry and reduced soot concentrations (and thus reduced continuum radiation heat losses from soot).

Present optical measurements of soot volume fractions are in excellent agreement with recent gravimetric measurements of soot vol-

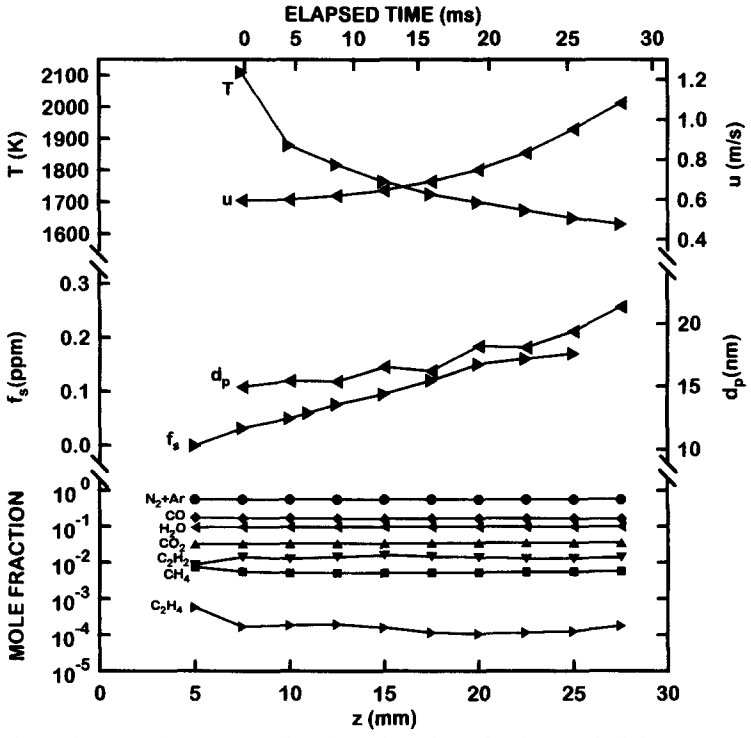

Fig. 3. Soot and flame properties along the axis of the C/O = 0.78 flame.

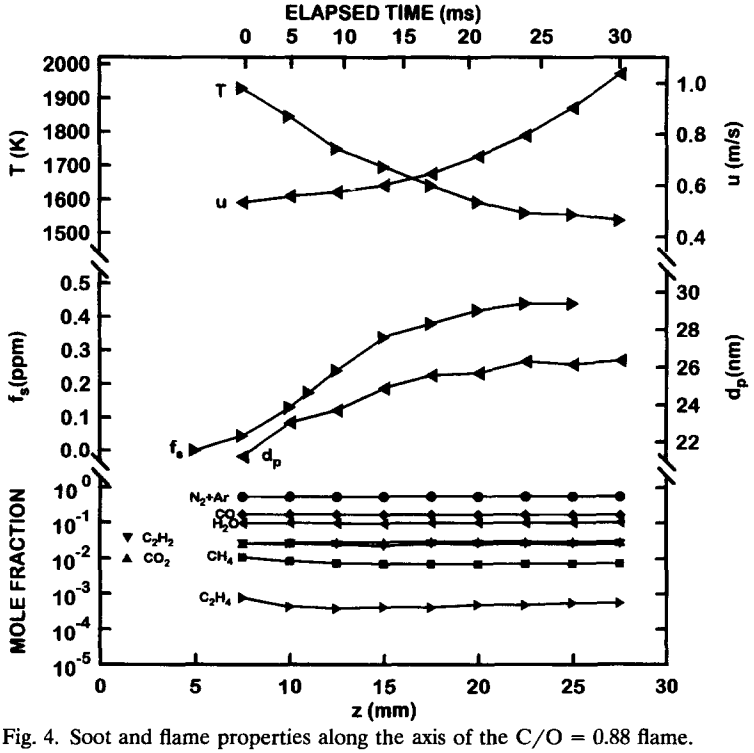

Fig. 4. Soot and flame properties along the axis of the C/O = 0.88 flame.

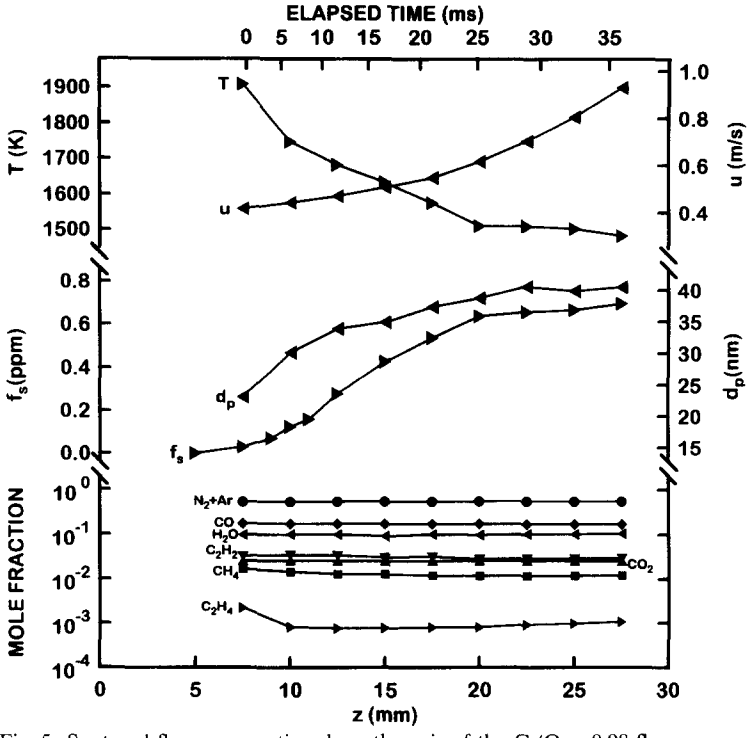

Fig. 5. Soot and flame properties along the axis of the C/O = 0.98 flame.

ume fractions; this includes the measurements of Benish et al. [28] for a C/O = 0.79 compared to present results for a C/O = 0.78 in Fig. 3 and present gravimetric measurements for C/O = 0.78 and 0.88 to be discussed later. The results of Harris and Weiner [11] for a C/O = 0.79 are nearly three times larger than the results of Benish et al. [28] and the present investigation, for reasons that have not been explained. Finite soot volume fractions are first observed near $z = 7.5$ mm for the three test flames in Figs. 3–5. Soot volume fractions subsequently increase but then level off with increasing distance from the burner exit, which is a well-known trend for soot-containing laminar premixed flames [4, 11].

Present measurements of primary soot particle diameters for C/O = 0.78 in Fig. 3, are comparable to the recent measurements of Benish et al. [28] for a similar flame having a C/O = 0.79 and using similar methods. The range of present primary particle diameter measurements corresponds to conditions where soot volume fractions could be measured with acceptable experimental uncertainties and involves mean primary particle diameters generally larger than 10 nm. Smaller values of mean primary particle diameters can be found nearer to the onset of soot formation, where mean primary particle diameters increase rapidly with increasing streamwise distance. In the range of the measurements, mean primary particle diameters increase and then level off with increasing distance from the burner exit, similar to soot volume fractions.

Concentrations of major gas species are also plotted in Figs. 3–5. Where they overlap, present measurements are in good agreement with other results for these flame conditions, e.g., present C_2H_2 and CH_4 concentrations agree with those reported by Harris and Weiner [11] and Benish et al. [28] within experimental uncertainties. The concentrations of major gas species are nearly constant throughout the soot-formation region (the main exceptions are a slight reduction of the concentrations of C_2H_4 and a slight increase of the concentrations of C_2H_2 seen in the region $z = 5$–10 mm). This behavior is similar to the observations of Harris and Weiner [11] for comparable premixed ethylene/air flames at atmospheric pressure. These results indicate that rates of

soot formation in premixed flames do not decrease due to consumption of soot-forming hydrocarbon species similar to diffusion flames [1–3]; instead, subsequent results will show that this behavior can be explained as a result of reduced flame temperatures with increasing distance from the burner exit.

The volume fractions of CHS and soot along the axes of flames having C/O = 0.78 and 0.88 are plotted as a function of height above the burner exit in Fig. 6. Both optical and gravimetric determinations of soot volume fractions are illustrated. The agreement between these two determinations is within experimental uncertainties, thus alleviating concerns that variations of the refractive indices of soot with residence time in flame environments (due to soot dehydrogenation) might impair optical measurements of soot-formation rates. D'Alessio and co-workers [31, 32] also observe agreement between optical and gravimetric measurements of soot concentrations in laminar premixed flames at atmospheric pressure.

Present observations of CHS behavior illustrated in Fig. 6 also are qualitatively similar to the observations of D'Alessio and co-workers [31, 32]. The concentrations of CHS exhibit little variation in the soot-formation region in spite of significant increases of soot concentrations. This behavior is noteworthy because concentrations of CHS and soot follow similar trends in the soot inception region of premixed flames [31], and concentrations of both CHS and soot increase with C/O ratio for present test conditions. Taking the mean molecular weight of CHS to be 276 kg/kg-mol implies CHS volume fractions on the order of 10^{-4} for both the present flames and those of D'Alessio and co-workers [31, 32]; maximum soot volume fractions tend to be roughly 10^{-3} times smaller than those of CHS for both the present flames and those of D'Alessio and co-workers [31, 32].

Present measurements were used to study soot growth and nucleation in premixed flames, analogous to earlier study of these properties in diffusion flames [1–3]. Major assumptions of this analysis were similar to earlier work [1–3], as follows: soot surface growth, rather than soot nucleation, dominates soot mass production; effects of thermophoresis and diffusive soot motion are small, so that soot particles convect along the axis with the local gas velocity; and the surface area available for soot growth was equivalent to that of constant diameter spherical primary soot particles that meet at a point. This implies that the soot surface area per unit volume S can be found from

$$S = \pi d_p^2 n_p = 6 f_s / d_p, \tag{2}$$

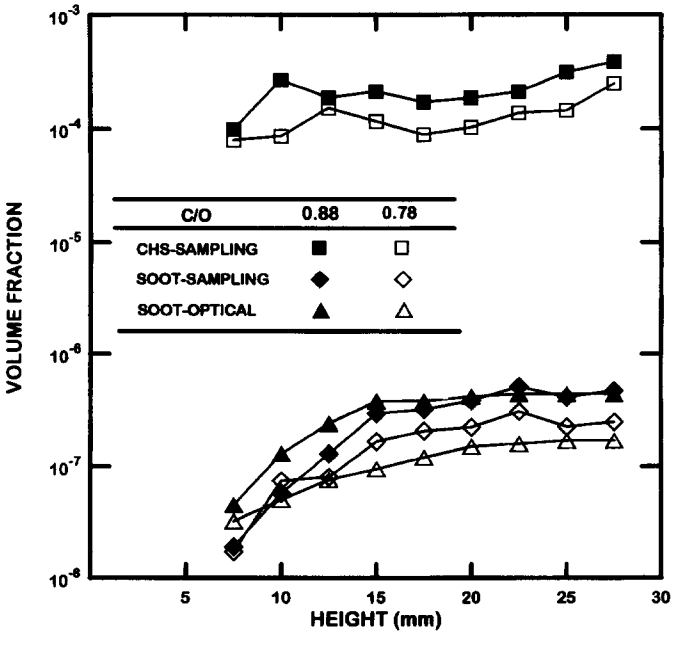

Fig. 6. Volume fractions of CHS and soot along the axes of the C/O = 0.78 and 0.88 flames.

where the last equality follows from Eq. 1. Then defining the soot growth rate w_g as the rate of increase of soot mass per unit area of soot surface and time, conservation of soot mass along a streamline under the previous assumptions yields

$$w_g = (\rho/S)d(\rho_s f_s/\rho)/dt. \quad (3)$$

The gas density in Eq. 3 was found from the present concentration and temperature measurements, assuming an ideal gas mixture of the major gas species and neglecting the volume of soot (which was only present at ppm levels). The soot density in Eq. 3 was taken to be 1850 kg/m^3 as before [1–3]. Finally, the temporal derivative in Eq. 3 was found from three-point least-squares fits of the argument of the derivative $\rho_s f_s/\rho$, similar to past work [1–3].

The soot nucleation rate was defined as the rate of increase of the number of primary soot particles per unit volume and time, similar to past work [1–3]. This definition is useful because the number of primary soot particles per unit volume is an important observable property of a soot-containing environment that affects the surface area available for soot growth as well as the optical and radiative properties of the flow. Nevertheless, it should be recognized that the present primary soot particle nucleation rate represents a composite of chemical and physical effects, e.g., the various chemical steps that eventually form large molecular weight hydrocarbon molecules as well as the subsequent physical coalescence of these substances to eventually form visible primary soot particles. Based on the same assumptions used to determine soot growth rates from Eq. 3, the expression for primary soot particle nucleation rate is

$$w_n = \rho d(n_p/\rho)/dt. \quad (4)$$

The temporal derivative in Eq. 4 was found from three-point least-squares fits of the argument of the derivative n_p/ρ, as before [1–3].

The four above-derived properties—S, n_p, w_n, and w_g—along the axes of the C/O = 0.78, 0.88, and 0.98 flames are plotted as a function of height above the burner in Fig. 7. The soot surface area per unit volume S increases with increasing height above the burner. This differs from the observations for similar flames by Harris and Weiner [11], who concluded that S was relatively independent of distance from the burner exit, based on the assumption of Mie scattering for equivalent spheres (which is now known to be ineffective for describing soot optical properties [40–42]). The trend of increasing values of S with increasing propensity to soot (or C/O ratio) and maximum values of S in the range 50–100 m^{-1}, however, agree with the observations of Harris and Weiner [11] for comparable flame conditions.

Values of n_p illustrated in Fig. 7 initially increased rapidly with distance, but later leveled out similar to soot volume fractions. In fact, n_p even decreased somewhat at large distances from the burner exit for C/O = 0.98; this behavior actually implies unphysical negative nucleation rates attributable to experimental uncertainties in a region where rates of nucleation are small. In particular, negative nucleation rates for the present data cannot be attributed to aggregation of primary particles because soot aggregates are represented by touching spherical primary particles, not equivalent spheres as invoked in some studies. Finally, an interesting trend for n_p is that it actually decreases with propensity to soot (or increasing C/O ratio) for the present test conditions, contrary to the behavior of f_s and d_p. This behavior follows because larger radiative heat losses at larger C/O ratios cause flow temperatures to decrease (see Figs. 3–5), which reduces nucleation rates because they are relatively temperature-sensitive as discussed later (also see Refs. 1–3). The net effect is that the larger values of soot volume fractions at larger C/O ratios are accommodated by primary soot particles that have larger diameters but smaller concentrations.

Given the behavior of f_s and n_p that was just discussed, it is evident that both soot growth and nucleation rates progressively decrease with increasing distance from the burner exit, through Eqs. 3 and 4. This behavior is more directly indicated by the plots of w_n and w_g appearing in Fig. 7. As discussed earlier, values of w_n tend to decrease with increasing propensity to soot (or increasing C/O ratio). On the other hand, this behavior is compen-

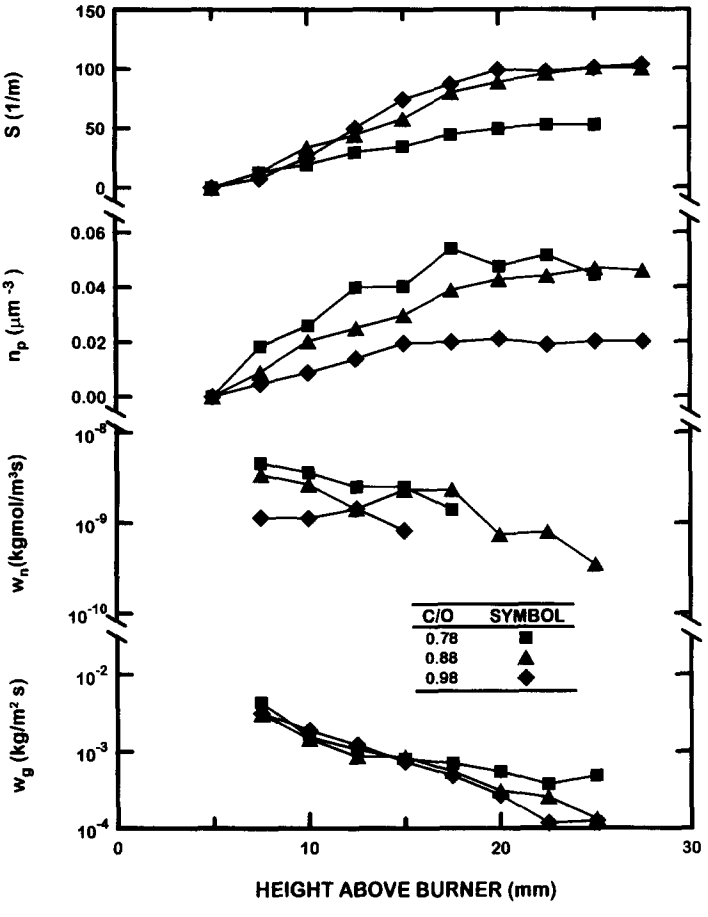

Fig. 7. Derived soot properties (S, n_p, w_n, and w_g) along the axes of the present flames.

sated by the increase of w_g with increasing propensity to soot (or increasing C/O ratio) so that large soot volume fractions and primary particle diameters are observed at large C/O ratios, as expected. Although present flame conditions are comparable to Harris and Weiner [11], present maximum values of w_g are somewhat larger, e.g., 0.002 as opposed to 0.0005 kg/m^{2}s, which is surprising because the Harris and Weiner [11] measurements overestimate soot volume fractions as discussed in connection with Fig. 3. These differences of maximum w_g are mainly caused by the different estimates of S as discussed in connection with Fig. 7.

Gas Species Concentrations

It is evident from Figs. 3–5 that the concentrations of major gas species exhibit little variation with distance within the soot-formation region of the present flames. On the other hand, it is of interest to examine the yields of major gas species as a function of C/O ratio because this highlights the gas species responsible for the growth and nucleation of soot. Measured concentrations of major gas species are plotted in Fig. 8 as a function of C/O ratio for the present flames along with predictions of these properties for the same flames based on the mechanisms of Frenklach and coworkers [33–35] and Leung and Lindstedt [46]. Both measurements and predictions are for z = 20 mm; however, these properties do not vary significantly with distance over the range of the present measurements, as noted earlier. Concentrations of nitrogen and argon have been summed for both measurements and predictions because these species eluted at the same time from the present chromatograph columns and were not distinguished during the measurements.

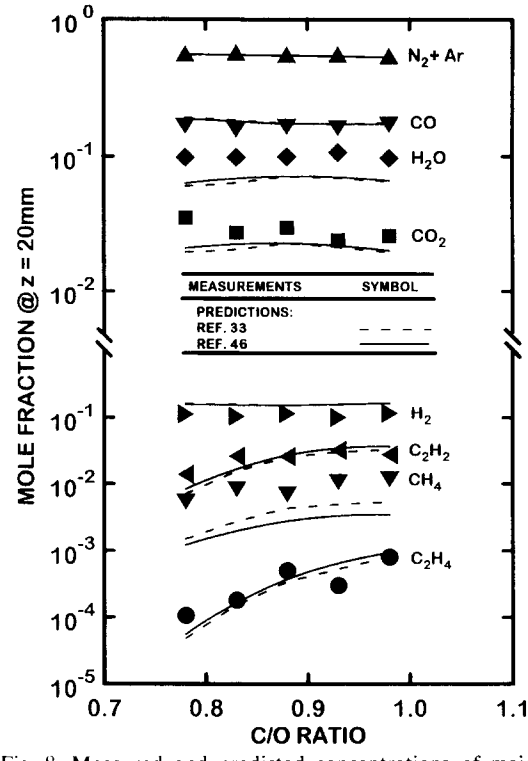

Fig. 8. Measured and predicted concentrations of major gas species at the axes of the present flames at z = 20 mm.

Soot volume fractions and CHS concentrations tend to increase with C/O ratio, with soot volume fractions tending to level out at large C/O ratios; for present test conditions, see Fig. 6. The corresponding variations of nonhydrocarbon species (N_2 + Ar, CO, H_2O, CO_2, and H_2) with variations of C/O ratio seen in Fig. 8 are modest by comparison. Concentrations of hydrocarbons potentially associated with the formation of soot and CHS exhibit a slight tendency to increase and then level out as C/O ratio increases, similar to soot volume fractions. Harris and Weiner [11] report mole fractions of C_2H_2 and CH_4 of roughly 2 and 1% at larger C/O ratios for premixed ethylene/air flames, also relatively independent of distance from the burner, which is in good agreement with present results. Similar to the observations of Harris and Weiner [11], acetylene is seen to be the dominant light hydrocarbon species present that is likely to contribute significantly to soot formation. Methane is the next most prevalent light hydrocarbon species, but its large H/C ratio does not suggest that it has a direct role in the formation of soot. Finally, the concentrations of ethylene, the third most prevalent light hydrocarbon species observed, are generally 2 orders of magnitude smaller than acetylene, which together with its relatively large H/C ratio does not suggest a major direct soot formation role for this species.

The predictions of the yields of major gas species using PREMIX with the mechanisms of Frenklach and co-workers [33–35] and Leung and Lindstedt [46] are also plotted in Fig. 8. Predictions using the two mechanisms are essentially the same. The comparison between measured and predicted species mole fractions is good in view of the complexity of the chemistry of the present flames. The major discrepancies are that predictions underestimate mole fractions of H_2O, CO_2, and CH_4, and overestimate those of H_2. Nevertheless, the differences between the predictions and measurements are comparable to experimental uncertainties. As a further test, predictions and measurements of major gas species were compared for the laminar premixed methane/oxygen flames at atmospheric pressure studied by Ramer et al. [18], finding agreement similar to the results illustrated in Fig. 8.

In view of the good predictions of major gas species mole fractions using the mechanisms of Frenklach and co-workers [33–35] and Leung and Lindstedt [46], these mechanisms were used to estimate radical concentrations in the present flames in order to help interpret measured soot growth properties. Predictions of the mole fractions of H for both of these models, along with estimates assuming local equilibrium for H (based on the thermochemical properties of Ref. 51 and the present measurements of H_2 concentrations and temperature) are illustrated in Fig. 9. Predictions using both mechanisms are essentially the same and are in good agreement with estimates based on the assumption of local thermodynamic equilibrium for H. The mole fractions of H_2 vary only slightly for present conditions (see Fig. 8); therefore, the variations of the mole fractions H are mainly due to variations of temperature. Thus, H mole fractions are largest at small z and C/O ratios where temperatures are largest. As suggested by Frenklach and Wang

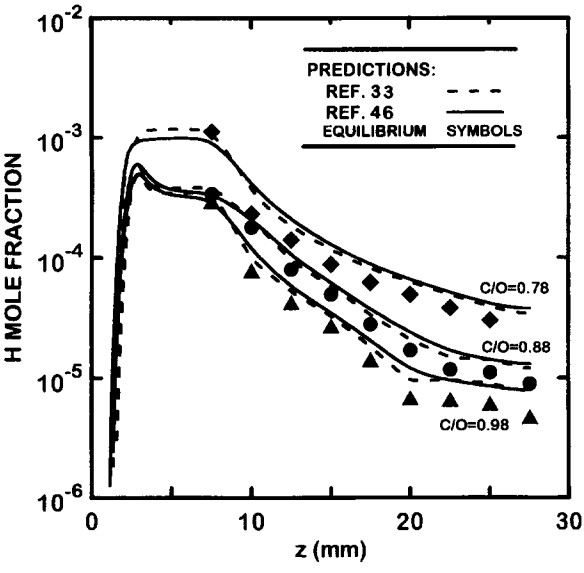

Fig. 9. Predicted H atom concentrations along the axes of the present flames.

[33], a similar correspondence between H atom mole fractions and soot surface growth rates (and thus temperatures and soot surface growth rates when variations of acetylene mole fractions are small) can be anticipated from the HACA mechanism of soot surface growth. This possibility will be considered subsequently.

Soot Surface Growth

In order to interpret the present soot surface growth rates, the gross growth rates obtained from Eq. 3 were corrected for effects of soot oxidation similar to past studies of soot surface growth rates in diffusion flames [1–3]. It was found that effects of soot oxidation were generally negligible except when soot growth rates became small at the most downstream locations considered during the present experiments. Soot oxidation by CO_2 and H_2O was estimated following Johnstone et al. [52] and Libby and Blake [53, 54], which gave results similar to Bradley et al. [55]. Soot oxidation by O_2 was not a factor because no O_2 was detected. Soot oxidation by OH was estimated as discussed by Neoh et al. [56], using present estimates of OH concentrations found from the PREMIX computations based on the mechanisms of Frenklach and co-workers [33–35] and Leung and Lindstedt [45]; however, it was found that direct oxidation of soot by OH was negligible even for collision efficiencies of unity. The final result was that CO_2 was the main potential source of soot oxidation for present conditions; nevertheless, soot oxidation rates never exceeded half the gross soot growth rates, even at the most downstream locations where data were reduced to obtain the results presented here. As a result, effects of current uncertainties about soot oxidation rates in fuel-rich environments should not have a large impact on findings concerning soot growth discussed in the following text.

Present soot surface growth rates were initially correlated similar to earlier work for diffusion flames [1–3] in order to obtain general comparisons with past measurements. This involved associating soot growth rates with acetylene concentrations similar to earlier work [1–4, 11–17]. Acetylene is a natural choice because its concentrations are large in soot-formation regions, because it has a low H/C ratio anticipated for soot-forming compounds, and because it assumes a dominant role in the HACA soot-formation mechanisms. Present soot growth rates, corrected for soot oxidation, are plotted as a function of acetylene concentration in Fig. 10. The plots of Fig. 10 also include earlier results from measurements in laminar premixed flames due to Bockhorn and co-workers [7–10], Harris and Weiner [11–14], and Ramer et al. [18], along with the earlier measurements in diffusion flames due to Sunderland and co-workers [1–3]. The axes of this

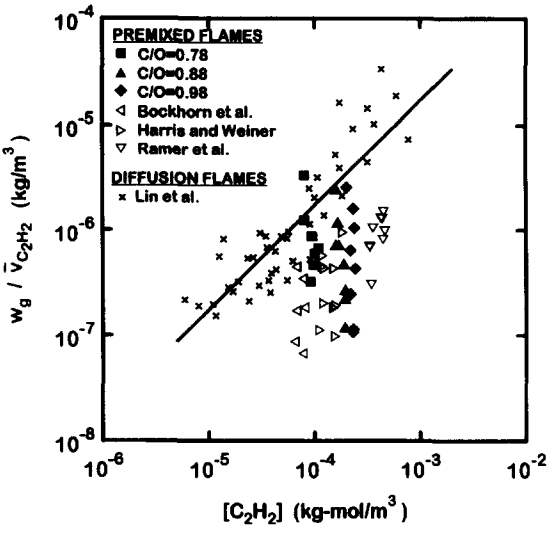

Fig. 10. Soot particle surface growth rates as a function of acetylene concentrations for laminar premixed and diffusion flames. Premixed flame data from Bockhorn and co-workers [7–10], Harris and Weiner [11–14], Ramer et al. [18], and the present investigation; diffusion flame data from Sunderland and co-workers [1–3]. The line shown on the figure is the best-fit correlation for soot growth in the diffusion flames of Refs. 1–3.

plot anticipate a simple acetylene collision efficiency for soot growth, similar to observations for acetylene diffusion flames [1–3], i.e.,

$$w_g = k_g(T)[C_2H_2]^n = \eta C_{C_2H_2}\bar{v}_{C_2H_2}[C_2H_2]/4. \quad (5)$$

The second equality of Eq. 5 is appropriate for a simple acetylene collisional growth mechanism where the surface reactivity for growth is constant and the reaction order with respect to acetylene is unity. Soot surface growth rates for diffusion flames, corrected for oxidation, yield a good correlation based on this approach with a collision efficiency of 0.39% [3].

In contrast to the surface growth rates for diffusion flames from Refs. 1–3, the premixed flame measurements illustrated in Fig. 10 are not correlated by an acetylene collisional growth mechanism. Nevertheless, the largest soot growth rates of premixed flames (observed for new soot near the start of the soot-formation region) are comparable to surface growth rates observed in Refs. 1–3 for diffusion flames. This agreement is closest for the present premixed flame measurements, where w_g was found using the same experimental methods and oxidation corrections as the diffusion flame measurements of Refs. 1–3. On the other hand, soot growth rates in all the premixed flames decrease with height above the burner, at nearly constant concentrations of acetylene and other hydrocarbons, thus exhibiting the effect of age mentioned earlier. This age effect is responsible for the vertical span of the data for premixed flames seen in Fig. 10. As a result, expressions similar to Eq. 5, that involve major species and CHS whose concentrations are relatively independent of distance from the burner exit in premixed flames, are not likely to provide generally effective correlations of soot surface growth rates.

Subsequent consideration of present soot surface growth rates emphasized HACA mechanisms [33–38] at the limit where growth was due to direct reactive addition of acetylene to the surface of growing soot particles rather than by reactive addition or coalescence of PAH. This approximation was considered as a first step for analyzing the present experiments due to the strong relationship between acetylene concentrations and soot growth rates observed for diffusion flames at similar conditions [1–3]. In addition, concentrations of acetylene are large compared to CHS (and even more so for PAH [31, 32]) for present test conditions (see Figs. 3–6), so that potential soot growth rates are almost an order of magnitude larger for acetylene than for PAH, given comparable collision/coalescence efficiencies. Furthermore, the computations of Frenklach and Wang [33] suggest a greater contribution of acetylene than PAH addition to soot surface growth rates for premixed ethylene-fueled flames at atmospheric pressure. On the other hand, the present approximation merits careful scrutiny in the future because Benish et al. [28] suggested a more dominate role for the PAH than for the acetylene mechanism for the present flame conditions, while the complete treatment of soot growth by Frenklach and co-workers [33–36] allowed for contributions from both the acetylene and PAH mechanisms.

The HACA mechanisms of soot surface growth due to Frenklach and co-workers [33–35], represented by the recent version of

Kazakov et al. [35] and Colket and Hall [37], were used to interpret the present measurements; they are representative of different approaches to treat effects of temperature on soot growth rates; see original sources for details. For present considerations, soot growth rates were corrected for effects of oxidation as described in connection with Fig. 10; therefore, oxidation reactions appearing in these HACA mechanisms were neglected. The resulting reaction mechanisms and rate constants for the Frenklach and co-workers [33–35] (as summarized by Kozakov et al. [35]) and Colket and Hall [37] methods are summarized in Tables 2 and 3, respectively. For these tables, C_s–H represents an armchair site, $C_s\cdot$ represents a corresponding radical site, and C_sCHĊH represents a radical/acetylene complex site on the soot particle surface. The net rate of soot particle surface growth was expressed, for both mechanisms, as

$$w_g = \alpha_i R_i, \tag{6}$$

where i = FW or CH denotes appropriate reaction parameters for the mechanisms of Frenklach and co-workers [33–35] and Colket and Hall [37], respectively. The parameter α_i is an empirical (steric) factor of order of magnitude unity that involves corrections when sites on carbon surfaces are treated analogous to corresponding sites on gaseous PAH molecules, while the R_i represent reaction rate expressions to be considered subsequently. Kazakov et al. [35] prescribe that α_{FW} is a function of the maximum temperature of the flame (see Table 2 for the correlation), while Colket and Hall [37] take α_{CH} to be a fixed constant. Adopting the steady-state approximation for fast reacting intermediates yields the expression for soot particle surface growth for the

TABLE 2

Summary of the Reaction Mechanism for Soot Particle Surface Growth (from Kazakov et al. [35])[a]

No.	Reaction	A (m, kg-mol, s)	n	E (kJ/kg-mol)
1	C_s–H + H → $C_s\cdot$ + H_2	2.5 (+11)	—	66,900
−1	$C_s\cdot$ + H_2 → C_s–H + H	3.9 (+9)	—	39,000
2	$C_s\cdot$ + H → C_s–H	1.0 (+11)	—	—
3	$C_s\cdot$ + C_2H_2 → C_s–H + H	8.4 (+8)	0.4	35,100

[a] Numbers in parentheses denote powers of 10. Definition of reaction rate coefficient $k = AT^n \exp(-E/(RT))$, while $[C_s\text{–H}] = 2.3(+19)$ sites/m^2, and $\alpha_{FW} = [\tanh(8168/T_{max} - 4.57) + 1]/2$ with T_{max} (K) and $C_{HACA} = 2M_c/A_v$ for present calculations.

[b] C_s–H represents an armchair site on the soot particle surface and $C_s\cdot$ represents the corresponding radical site.

TABLE 3

Summary of the Reaction Mechanism for Soot Particle Surface Growth (from Colket and Hall [37])[a]

No.	Reaction	A (m, kg-mol, s)	n	E (kJ/kg-mol)
1	C_s–H + H → $C_s\cdot$ + H_2	2.5 (+11)	—	50,200
−1	$C_s\cdot$ + H_2 → C_s–H + H	4.0 (+8)	—	29,300
2	$C_s\cdot$ + H → C_s–H	2.2 (+11)	—	—
−2	C_s–H → $C_s\cdot$ + H	2.0 (+17)	—	456,000
3	$C_s\cdot$ → C_2H_2 + products	3.0 (+14)	—	259,000
4	$C_s\cdot$ + C_2H_2 → C_sCHĊH	2.0 (+9)	—	16,700
−4	C_sCHĊH → $C_s\cdot$ + C_2H_2	5.0 (+13)	—	159,000
5	C_sCHĊH → C_s–H + H	5.0 (+10)	—	—

[a] Numbers in parentheses denote powers of 10. Definition of reaction rate coefficient is $k = AT^n \exp(-E/(RT))$, while $[C_s\text{–H}] = 2.3(+19)$ sites/m^2 and $\alpha_{CH} = 0.9$ and $C_{HACA} = 2M_c/A_v$ for present calculations.

[b] C_s–H represents an armchair site on the soot particle surface, $C_s\cdot$ represents the corresponding radical site, and C_sCHĊH represents a radical/acetylene complex site.

mechanism of Frenklach and co-workers [33–35],

$$R_{FW} = \frac{C_{HACA} k_1 k_3 [H][C_2H_2][C_s\text{–}H]}{k_{-1}[H_2] + k_2[H] + k_3[C_2H_2]}, \quad (7)$$

where $C_{HACA} = 2M_c/A_v$, while Frenklach and Wang [33] estimate $[C_s\text{–}H] = 2.3 \times 10^{19}$ sites/m^2. Proceeding in the same manner for the mechanism of Colket and Hall [37] yields

$$R_{CH} = \frac{C_{HACA}(k_1[H] + k_{-2})(k_4 k_5 [C_2H_2] - k_3(k_{-4} + k_5))[C_s\text{–}H]}{(k_{-1}[H_2] + k_2[H] + k_3)(k_{-4} + k_5) + k_4 k_5 [C_2H_2]}, \quad (8)$$

where C_{HACA} and $[C_s\text{–}H]$ are the same as before (note that Eq. 8 corrects some typographical errors and deletes some approximations for this equation in Ref. 37). The k_i in Eqs. 7 and 8 refer to the mechanisms summarized in Tables 2 and 3, respectively.

For present test conditions, the term involving the product $[H][C_2H_2]$ dominates the numerators and varies more than the denominators of Eqs. 7 and 8; therefore, the present oxidation-corrected soot growth rates are plotted in Fig. 11 as a function of [H], found assuming local thermodynamic equilibrium for H, in order to highlight the importance of the hydrogen abstraction portion of the HACA mechanism. The modest acetylene concentration variation over the present test range has been handled by normalizing w_g by $[C_2H_2]$ when plotting this figure. The resulting correlation between $w_g/[C_2H_2]$ and [H] is seen to be excellent. Noting the relationship between [H] and position illustrated in Fig. 9, and thus the relationship between [H] and temperature from the results illustrated in Figs. 3–5, it is strongly suggested that reduced soot surface growth rates with increasing residence time in premixed flames (aging) is caused by reduced temperatures through the HACA mechanism. Since continuum radiation from soot is primarily responsible for radiative heat losses in the present flames, this behavior implies that the presence of soot itself moderates rates of soot surface growth.

A more direct evaluation of the HACA mechanism of soot surface growth due to Frenklach and co-workers [33–35] was obtained by plotting w_g directly as a function of R_{FW} as indicated by Eqs. 6 and 7, using the equilibrium estimates of [H] as before. The upper part of Fig. 12 is an illustration of the

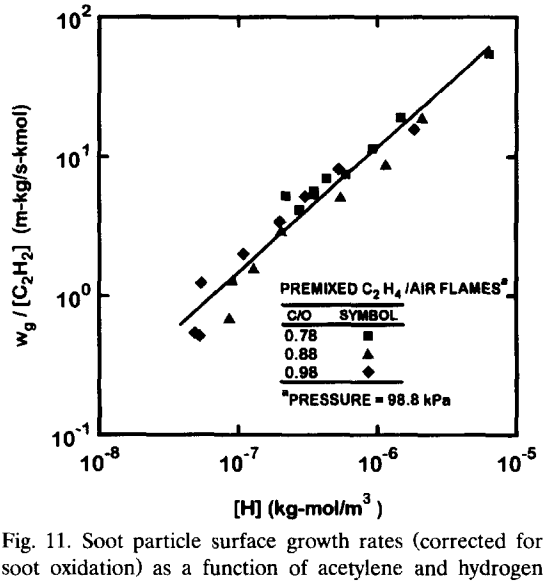

Fig. 11. Soot particle surface growth rates (corrected for soot oxidation) as a function of acetylene and hydrogen atom concentrations for the present flames. The line shown on the figure is the best-fit correlation of the present data when plotted in this manner.

strict use of the mechanism of Frenklach and co-workers [33–35], with $\alpha_{FW}(T)$ obtained from the correlation provided by Kazakov et al. [35], where the best fit correlation of the present measurements and the best fit of the HACA expression of Eqs. 6 and 7 are all plotted. Results from the HACA expression, with $\alpha_{FW}(T)$ obtained from Ref. 35, are seen to provide only a fair correlation of the measurements: the correlation yields best results when R_{FW} is large and temperatures approach the T_{max} conditions used to correlate $\alpha_{FW}(T)$, but the subsequent variation of w_g with R_{FW}, when temperatures decrease, is underestimated. This behavior suggests that the correlation of $\alpha_{FW}(T)$ with the local flame temperature might yield improved results, which also would be more physically appealing for a steric

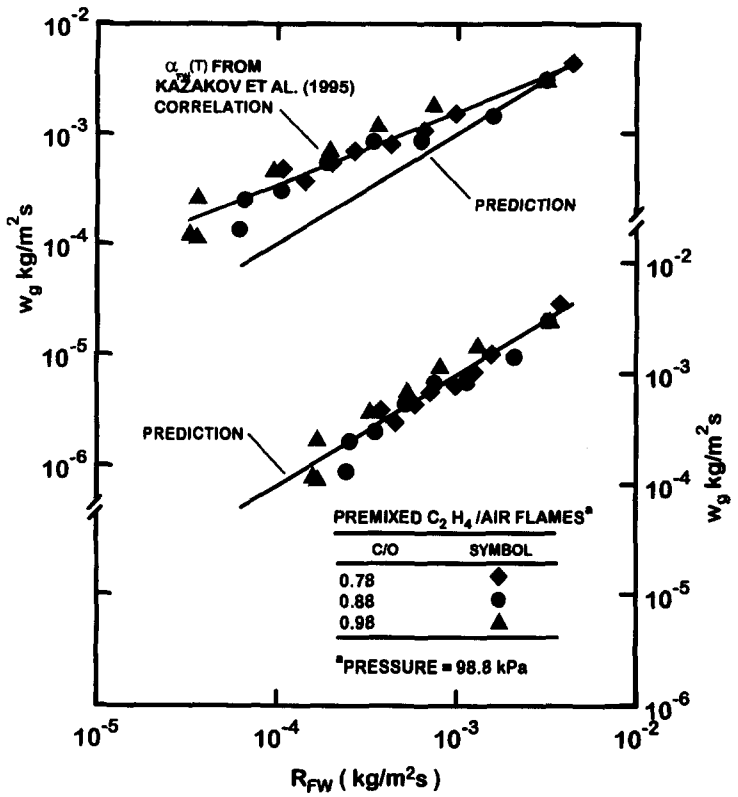

Fig. 12. Soot particle surface growth rates (corrected for soot oxidation) in terms of the HACA mechanism of Frenklach and co-workers [33–35] for the present flames. The upper figure illustrates results using the steric factor of Kazakov et al. [35]; the lower figure illustrates results using the present correlation of the steric factor.

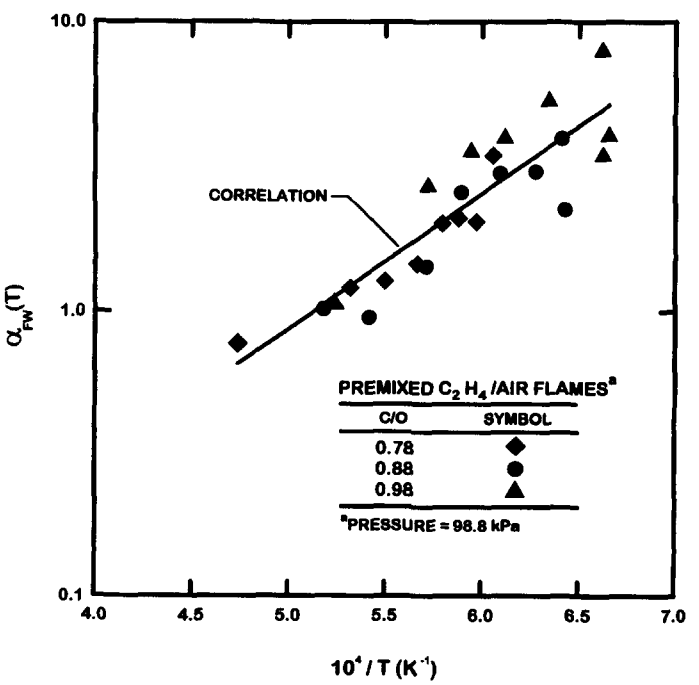

Fig. 13. Correlation of the steric factor of Frenklach and co-workers [33, 34] based on local temperatures for the present soot growth data. The line shown is the best-fit correlation of the data when plotted in this manner.

factor parameter in any event. The resulting correlation for $\alpha_{FW}(T)$, based on local temperatures while fitting present measurements for $\alpha_{FW}(T)$ to the HACA predictions, is illustrated in Fig. 13. These results indicate values of $\alpha_{FW}(T)$ near unity, which is anticipated for a parameter like $\alpha_{FW}(T)$, with values of $\alpha_{FW}(T)$ decreasing with increasing temperature, similar to the observations of Kazakov et al. [35]. The best fit expression for $\alpha_{FW}(T)$, also shown on the plot, was found to be

$$\alpha_{FW}(T) = 0.004 \exp(10800/T) \quad (9)$$

with $T(K)$. Finally, if the correlation of Eq. 9 is used in Eqs. 6 and 7 to find w_g, the results shown in the lower part of Fig. 12 are obtained. It is evident that these predictions now provide an excellent correlation of the present measurements, with all parameters of α_{FW} and R_{FW} based on local conditions within the flames.

The corresponding evaluation of the HACA mechanism of soot surface growth due to Colket and Hall [37], finding [H] using equilibrium estimates as before, is illustrated in Fig. 14. In this case, the HACA mechanism provides a good correlation of the measurements with a best fit value of $\alpha_{CH} = 0.9$ with an uncertainty (95% confidence) of 0.2. Thus, this approach also yields a value of α_{CH} on the order of unity as anticipated, with the mechanism also supplying a reasonably good representation of effects of temperature while using a constant steric factor.

The evaluations of the HACA mechanisms of Frenklach and co-workers [33–35] and Colket and Hall [37] discussed in connection with Figs. 12–14 are quite encouraging, and mechanisms similar to these methods may provide the basis of a reasonably general treatment of soot surface growth. Nevertheless, more work is needed to evaluate these methods over a wider range of test conditions, to resolve the relative contributions of acetylene and PAH to soot surface growth, to properly incorporate effects of simultaneous soot oxidation from all soot-oxidizing species present in the system, and to firmly establish the individual reaction steps of the soot surface growth mechanism.

Soot Nucleation

Present measurements of soot nucleation rates were based on primary soot particle formation rates and were correlated in terms of acetylene concentrations, similar to earlier studies of soot

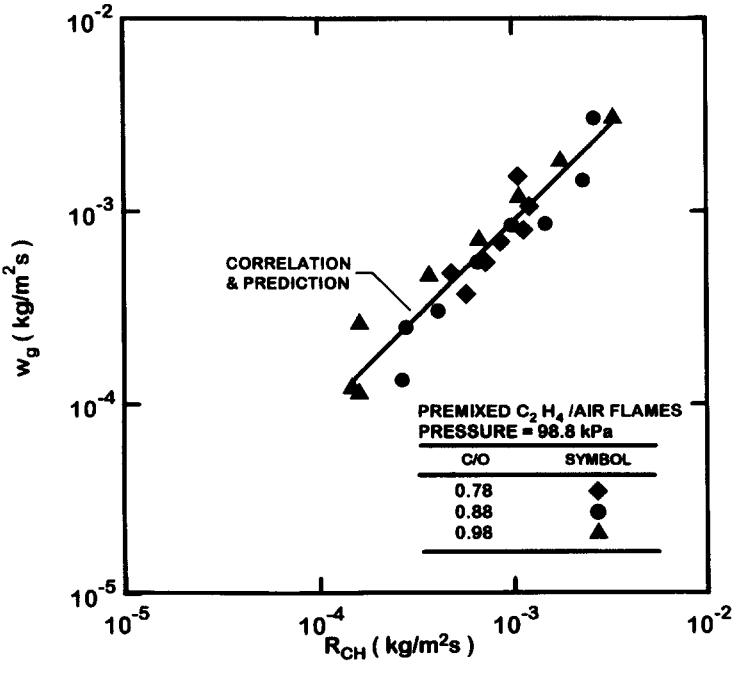

Fig. 14. Soot particle surface growth rates (corrected for soot oxidation) in terms of the HACA mechanism of Colket and Hall [37] for the present flames.

nucleation in diffusion flames [1–3, 45], i.e.,

$$w_n = k_n(T)[C_2H_2]^n, \quad (10)$$

where $k_n(T)$ is an Arrhenius expression. Similar to earlier findings [1–3], measurements indicated that first-order behavior was reasonable, although the rather narrow range of present acetylene concentrations precluded an accurate determination of the reaction order with respect to acetylene; see Figs. 3–5 and 8.

The present primary soot particle nucleation rate measurements are plotted in Fig. 15 as a function of temperature, assuming first-order kinetics with respect to acetylene. Recent results for diffusion flames, also assuming first-order kinetics with respect to acetylene, are plotted in the figure as well. The diffusion-flame results include the findings of Sunderland and co-workers [1–3], using experimental methods similar to the present investigation, and the correlation of Leung et al. [45], based on earlier measurements. The differences between the correlations of Sunderland and co-workers [1–3] and Leung et al. [45] are discussed in Ref. 1. The scatter of primary soot particle nucleation rate data from both the present study and Refs. 1–3 is appreciable due to the strong sensitivity of n_p to d_p through Eq. 1.

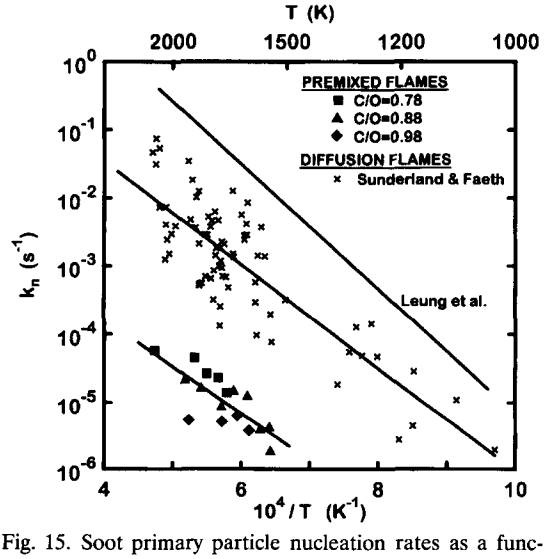

Fig. 15. Soot primary particle nucleation rates as a function of temperature for laminar premixed and diffusion flames. Premixed flame data from the present investigation; diffusion flame data from Sunderland and co-workers [1–3] and Leung et al. [45]. The lines shown represent the best-fit correlation of the measurements for the present premixed flames, the diffusion flame measurements of Sunderland and co-workers [1–3], and the results considered by Leung et al. [45].

Effects of temperature on w_n were nearly the same for the present premixed flames and the diffusion flames of Refs. 1–3. Thus, based on the units w_n (kg-mol/m^3 s), $[C_2H_2]$ (kg-mol/m^3), and $T(K)$, the present premixed-flame primary soot particle nucleation rates can be correlated as

$$w_n = 0.064[C_2H_2]\exp(-16100/T), \quad (11)$$

which is shown on the plot of Fig. 15. The range of present data used to find Eq. 11 is as follows: acetylene concentrations of $5–24 \times 10^{-5}$ kg-mol/m^3, temperatures of 1500–2200 K, and $k_n = 10^{-6}–10^{-4}$ s^{-1}. The corresponding correlation for the acetylene/air diffusion flame measurements of Ref. 2 is (note that the results of Refs. 1 and 3 are similar)

$$w_n = 37.9[C_2H_2]\exp(-17500/T), \quad (12)$$

which is also shown on the plot. The range of data used to find Eq. 12 is as follows: acetylene concentrations of $6 \times 10^{-6}–1 \times 10^{-3}$ kg-mol/m^3, temperatures of 1000–2100 K, and $k_n = 10^{-6}–10^{-2}$ s^{-1}. Thus, the ranges of the dependent variables for the diffusion flames span the corresponding ranges for the premixed flames. The standard deviation of the activation temperature for Eq. 11 is 1340 K. Finally, the corresponding activation energy of Eq. 11 is 11,100 kJ/kg-mol (32 kcal/gm-mol), which is modest but not unreasonable for a condensation-like process such as nucleation. In particular, present primary soot particle nucleation rates involve both chemical effects, which cause large molecular weight hydrocarbon species to form and physical effects of coalescence of these substances to subsequently form visible primary soot particles, as discussed earlier. It is well known that combining such chemical and physical phenomena into single Arrhenius expressions similar to Eqs. 11 and 12 yield reduced temperature dependence (or apparent activation energies) compared with values appropriate for the chemical processes alone.

An important feature of the primary soot particle nucleation rate results illustrated in Fig. 15 involves the much smaller nucleation rates observed for the premixed flames than for the diffusion flames at otherwise comparable conditions. This shortfall of soot nucleation rates in premixed flames even exceeds that of the growth rates illustrated in Fig. 10. A satisfactory explanation of this behavior must consider the complexities of the PAH, acetylene, and dehydrogenation reactions, and processes of coalescence, that finally yield observable primary soot particles.

CONCLUSIONS

Flame structure and soot processes were studied in laminar premixed ethylene/air flames at atmospheric pressure for conditions similar to those considered by Harris and Weiner [11], e.g., C/O ratios in the range 0.78–0.98. The test conditions involved acetylene concentrations of $5–24 \times 10^{-5}$ kg-mol/m^3, temperatures of 1500–2200 K, and soot concentrations up to roughly 1 ppm. The major conclusions of the study are as follows:

1. Present measurements agreed with many observations of Harris and Weiner [11] for comparable conditions except that present maximum soot volume fractions were one-third as large, that present soot surface area per unit volume increased with residence time rather than remaining constant, and that present maximum soot growth rates were roughly four times larger in spite of lower soot volume fraction values. Reasons for the different soot volume fractions are not known; the other differences are due to the present improved measurements of soot structure and flow residence times. In addition, present measurements are in good agreement with those of Benish et al. [28] for similar flames, where these measurements overlap.
2. Present soot surface growth rates of new soot in premixed flames were comparable to recent observations of soot surface growth rates in diffusion flames using similar experimental methods [1–3]. Contrary to behavior in diffusion flames, but similar to past observations in premixed flames [7–32], soot growth rates decreased with increasing residence time (an apparent effect of age) in spite of the continued availability of acetylene. This behavior is attributed to reduced concentrations of H needed to activate sites for carbon addition for both gaseous hydrocarbon molecules and soot particle surfaces, according to HACA mechanisms. In turn, the reduction of H was caused by reductions of temperature that were largely due to continuum radiation from soot; therefore, the presence of soot itself acts to moderate the rate of growth of soot.
3. Present measurements of soot surface growth rates, corrected for oxidation, were in reasonably good agreement with estimates based on direct reactive addition of acetylene to the surface of soot particles using the hydrogen-abstraction/carbon-addition (HACA) mechanisms of both Frenklach and co-workers [33–35] and Colket and Hall [37]. Nevertheless, more work is needed to evaluate the HACA mechanisms over broader parameter ranges, to resolve effects of the relative contributions of reactive coalescence of PAH and acetylene to soot surface growth, to incorporate effects of simultaneous surface oxidation of soot during surface growth, and to assess the individual reaction steps in the surface growth rate mechanism.
4. Predictions of the yields of major gas species using PREMIX, based on the mechanisms of Frenklach and co-workers [33–35] and Leung and Lindstedt [46], were in good agreement with present measurements for premixed ethylene/air flames at atmospheric pressure, and with earlier measurements of Ramer et al. [18] for premixed methane/oxygen flames at atmospheric pressure. In addition, predictions of the concentrations of H were nearly identical for both mechanisms and agreed with estimates based on local H equilibrium throughout the soot formation region. These indicate good capabilities for estimating the environment of soot formation processes in premixed flames at atmospheric pressure when temperatures are known.
5. Primary soot particle nucleation in the present premixed flames was roughly first order

with respect to acetylene concentrations with a modest activation energy of 11,100 kJ/kg-mol (32 kcal/gm-mol), which agrees reasonably well with recent observations for diffusion flames [1–3]; however, present primary soot particle nucleation rates for premixed flames were roughly 2 orders of magnitude smaller than the observations in diffusion flames at comparable conditions [1–3], for reasons that still must be explained.

This research was sponsored by NASA Grant NAG3-1245 under the technical management of D. L. Urban of the NASA Lewis Research Center, and Office of Naval Research Grant No. N00014-93-0321 under the technical management of G. D. Roy. The authors would like to acknowledge useful input from M. B. Colket and M. Frenklach concerning soot surface growth mechanisms.

REFERENCES

1. Sunderland, P. B., Köylü, Ü. Ö., and Faeth, G. M., *Combust. Flame* 100:310 (1995).
2. Sunderland, P. B., and Faeth, G. M., *Combust. Flame* 105:132 (1996).
3. Lin, K.-C., Sunderland, P. B., and Faeth, G. M., *Combust. Flame* 104:369 (1996).
4. Haynes, B. S., and Wagner, H. G., *Prog. Energy Combust. Sci.* 7:229 (1981).
5. Glassman, I., *Twenty-Second Symposium (International) on Combustion*, The Combustion Institute, Pittsburgh, 1988, p. 295.
6. Howard, J. B., *Twenty-Third Symposium (International) on Combustion*, The Combustion Institute, Pittsburgh, 1990, p. 1107.
7. Bockhorn, H., Fetting, F., Wannemacher, G., and Wentz, H. W., *Nineteenth Symposium (International) on Combustion*, The Combustion Institute, Pittsburgh, 1982, p. 1413.
8. Bockhorn, H., Fetting, F., Heddrich, A., and Wannemacher, G., *Twentieth Symposium (International) on Combustion*, The Combustion Institute, Pittsburgh, 1984, p. 979.
9. Wieschnowsky, U., Bockhorn, H., and Fetting, F., *Twenty-Second Symposium (International) on Combustion*, The Combustion Institute, Pittsburgh, 1988, p. 343.
10. Mauss, F., Schäfer, T., and Bockhorn, H., *Combust. Flame* 99:697 (1994).
11. Harris, S. J., and Weiner, A. M., *Combust. Sci. Technol.* 31:155 (1983).
12. Harris, S. J., and Weiner, A. M., *Combust. Sci. Technol.* 32:267 (1983).
13. Harris, S. J., and Weiner, A. M., *Combust. Sci. Technol.* 38:75 (1984).
14. Harris, S. J., and Weiner, A. M., *Twentieth Symposium (International) on Combustion*, The Combustion Institute, Pittsburgh, 1984, p. 969.
15. Harris, S. J., *Combust. Flame* 66:211 (1986).
16. Harris, S. J., Weiner, A. M., Blint, R. J., and Goldsmith, J. E. M., *Twenty-First Symposium (International) on Combustion*, The Combustion Institute, Pittsburgh, 1986, p. 1033.
17. Harris, S. J., and Weiner, A. M., *Twenty-Second Symposium (International) on Combustion*, The Combustion Institute, Pittsburgh, 1988, p. 333.
18. Ramer, E. R., Merklin, J. F., Sorensen, C. M., and Taylor, T. W., *Combust. Sci. Technol.* 48:241 (1986).
19. Mätzing, H., and Wagner, H. Gg., *Twenty-First Symposium (International) on Combustion*, The Combustion Institute, Pittsburgh, 1986, p. 1047.
20. Böhm, H., Hesse, D., Jander, H., Lüers, B., Pietscher, J., Wagner, H. Gg., and Weiss, M., *Twenty-Second Symposium (International) on Combustion*, The Combustion Institute, Pittsburgh, 1988, p. 403.
21. Böhnig, M., Feldermann, Chr., Jander, H., Lüers, B., Rudolph, G., and Wagner, H. Gg., *Twenty-Third Symposium (International) on Combustion*, The Combustion Institute, Pittsburgh, 1990, p. 1581.
22. Böhm, H., Feldermann, Chr., Heidermann, Th., Jander, H., Lüers, B., and Wagner, H. Gg., *Twenty-Fourth Symposium (International) on Combustion*, The Combustion Institute, Pittsburgh, 1992, p. 991.
23. Hanisch, S., Jander, H., Pape, Th., and Wagner, H. Gg., *Twenty-Fifth Symposium (International) on Combustion*, The Combustion Institute, Pittsburgh, 1994, p. 577.
24. Lam, F. W., Howard, J. B., and Longwell, J. P., *Twenty-Second Symposium (International) on Combustion*, The Combustion Institute, Pittsburgh, 1988, p. 323.
25. Lam, F. W., Longwell, J. P., and Howard, J. B., *Twenty-Third Symposium (International) on Combustion*, The Combustion Institute, Pittsburgh, 1990, p. 1477.
26. McKinnon, J. T., and Howard, J. B., *Twenty-Fourth Symposium (International) on Combustion*, The Combustion Institute, Pittsburgh, 1992, p. 965.
27. Lefleur, A. L., Howard, J. R., Taghizadeh, K., Plummer, B., Scott, L. T., Necula, A., and Swallow, K. C., *J. Phys. Chem.*, in press.
28. Benish, T. G., Lafleur, A. L., Taghizadeh, K., and Howard, J. B., *Twenty-Sixth Symposium (International) on Combustion*, The Combustion Institute, Pittsburgh, in press.
29. Macadam, S., Hoffman, A. B., Beér, J. M., and Sarofim, A. F., *Twenty-Sixth Symposium (International) on Combustion*, The Combustion Institute, Pittsburgh, in press.
30. Smedley, J. M., Williams, A., and Bartle, K. D., *Combust. Flame* 91:71 (1992).
31. D'Alessio, A., D'Anna, A., D'Orsi, A., Minutolo, P., Barbella, R., and Ciajolo, A., *Twenty-Fourth Sympo-*

sium (International) on Combustion, The Combustion Institute, Pittsburgh, 1992, p. 973.
32. D'Anna, A., D'Alessio, A., and Minutolo, P., in *Soot Formation in Combustion* (H. Bockhorn, Ed.), Springer-Verlag, Berlin, 1994, p. 83.
33. Frenklach, M., and Wang, H., *Twenty-Third Symposium (International) on Combustion*, The Combustion Institute, Pittsburgh, 1990, p. 1559.
34. Frenklach, M., and Wang, H., in *Soot Formation in Combustion* (H. Bockhorn, Ed.), Springer-Verlag, Berlin, 1994, p. 165.
35. Kazakov, A., Wang, H., and Frenklach, M., *Combust. Flame* 100:111 (1995).
36. Frenklach, M., *Twenty-Sixth Symposium (International) on Combustion*, The Combustion Institute, Pittsburgh, in press.
37. Colket, M. B., and Hall, R. J., in *Soot Formation in Combustion* (H. Bockhorn, Ed.), Springer-Verlag, Berlin, 1994, p. 442.
38. Mauss, F., Trilken, B., Breitbach, H., and Peters, N., in *Soot Formation in Combustion* (H. Bockhorn, Ed.), Springer-Verlag, Berlin, 1994, p. 325.
39. Wersborg, B. L., Howard, J. B., and Williams, G. C., *Fourteenth Symposium (International) on Combustion*, The Combustion Institute, Pittsburgh, 1972, p. 929.
40. Köylü, Ü. Ö., and Faeth, G. M., *J. Heat Transfer* 115:409 (1993).
41. Köylü, Ü. Ö., and Faeth, G. M., *J. Heat Transfer* 116:152 (1994).
42. Köylü, Ü. Ö., and Faeth, G. M., *J. Heat Transfer* 116:971 (1994).
43. Dobbins, R. A., and Megaridis, C. M., *Langmuir* 3:254 (1987).
44. Rosner, D. E., Mackowski, D. W., and Garcia-Ybarra, P., *Combust. Sci. Technol.* 80:87 (1991).
45. Leung, K. M., Lindstedt, R. P., and Jones, W. P., *Combust. Flame* 87:289 (1991).
46. Leung, K. M., and Lindstedt, R. P., *Combust. Flame* 102:129 (1995).
47. Dalzell, W. H., and Sarofim, A. F., *J. Heat Transfer* 91:100 (1969).
48. Wu, J.-S., Krishnan, S. K., and Faeth, G. M., *J. Heat Transfer*, to appear.
49. Dobbins, R. A., Fletcher, R. A., and Lee, W., *Combust. Flame* 100:301 (1995).
50. Stein, S. E., and Fahr, A., *J. Phys. Chem.* 89:3714 (1985).
51. Kee, R. J., Grcar, J. F., Smooke, M. D., and Miller, J. A., *A Fortran Program for Modeling Steady Laminar One-Dimensional Premixed Flames*, Sandia National Laboratories Report No. SAND85-8240, 1985.
52. Johnstone, J. F., Chen, C. Y., and Scott, D. S., *Ind. Eng. Chem.* 44:1564 (1952).
53. Libby, P. A., and Blake, T. R., *Combust. Flame* 36:139 (1979).
54. Libby, P. A., and Blake, T. R., *Combust. Flame* 41:123 (1981).
55. Bradley, D., Dixon-Lewis, G., El-Din Habik, S., and Mushi, E. M. J., *Twentieth Symposium (International) on Combustion*, The Combustion Institute, Pittsburgh, 1984, p. 931.
56. Neoh, K. G., Howard, J. B., and Sarofim, A. F., in *Particulate Carbon* (D. C. Siegla and B. W. Smith, Eds.), Plenum Press, New York, 1980, pp. 261–277.